Translational Science

Cancer Research

Modulation of Macropinocytosis-Mediated Internalization Decreases Ocular Toxicity of Antibody–Drug Conjugates

Hui Zhao, John Atkinson, Sara Gulesserian, Zhilan Zeng, Jenny Nater, Jimmy Ou, Peng Yang, Karen Morrison, Jeffrey Coleman, Faisal Malik, Pia Challita-Eid, Sher Karki, Hector Aviña, René Hubert, Linnette Capo, Josh Snyder, Sung-Ju Moon, Roland Luethy, Brian A. Mendelsohn, David R. Stover, and Fernando Doñate

Abstract

AGS-16C3F is an antibody–drug conjugate (ADC) against ectonucleotide pyrophosphatase/phosphodiesterase 3 (ENPP3) containing the mcMMAF linker-payload currently in development for treatment of metastatic renal cell carcinoma. AGS-16C3F and other ADCs have been reported to cause ocular toxicity in patients by unknown mechanisms. To investigate this toxicity, we developed an *in vitro* assay using human corneal epithelial cells (HCEC) and show that HCECs internalized AGS-16C3F and other ADCs by macropinocytosis, causing inhibition of cell proliferation. We observed the same mechanism for target-independent internalization of AGS-16C3F in fibroblasts and human umbilical vein endothelial cells (HUVEC). Macropinocytosis-mediated intake of macromolecules is facilitated by the presence of positive charges or hydrophobic residues on the surface of the macromolecule. Modification of AGS-16C3F, either by attachment of polyglutamate peptides, mutation of residue K16 to D on AGS-16C3F [AGS-16C3F(K16D)], or decreasing the overall hydrophobicity via attachment of polyethylene glycol moieties, significantly reduced cytotoxicity against HCECs and other primary cells. Rabbits treated with AGS-16C3F showed significant ocular toxicity, whereas those treated with AGS-16C3F(K16D) presented with less severe and delayed toxicities. Both molecules displayed similar antitumor activity in a mouse xenograft model. These findings establish a mechanism of action for target-independent toxicities of AGS-16C3F and ADCs in general, and provide methods to ameliorate these toxicities.

Significance: These findings reveal a mechanism for nonreceptor-mediated toxicities of antibody drug conjugates and potential solutions to alleviate these toxicities. *Cancer Res; 78(8); 2115–26.* ©*2018 AACR.*

Introduction

The clinical utility of antibody–drug conjugates (ADC) is based on the concept of differential expression of antigens between tumor and normal tissues that allows for the specific delivery of chemotherapy to the tumor (1). Thus, toxicities of ADCs in humans were expected to have been related to levels of normal expression of the antigen for which the ADC is directed against. However, for most ADCs, approved or in clinical development, the reported toxicities have been mainly independent of the target (2–4). Some of the most common target independent toxicities for ADC containing auristatins or maytansinoids are ocular toxicity, thrombocytopenia, neuropathy, and neutropenia. Cleavage of the Val-Cit peptide bond in the linker by proteases secreted by differentiating neutrophils and release of monomethyl auristatin E (MMAE) has been proposed by our group to contribute to neutropenia for this type of ADC (5). Moreover, ADC internalization by macropinocytosis in differentiating megakaryocytes has been recently proposed by our group to contribute to thrombocytopenia induced by AGS-16C3F (6).

Several ADCs have been reported to cause reversible ocular toxicity in humans described as blurred vision and/or dry eye, which, upon examination, have been attributed to damage to the cornea leading to dose reductions in some cases (3, 7). These toxicities have been observed for ADCs against different targets such as ectonucleotide pyrophosphatase/phosphodiesterase 3 (ENPP3; ref. 8), CD19 (9), CD70 (10), HER2 (11, 12), mesothelin (13), folate receptor (14), CA9 (7), and 5T4 (15), none of which is known to be expressed in the cornea, except HER2 (16). More recently, corneal toxicities were observed in non-human primates (NHP) treated with an ADC against CDH6 containing an N-Succinimidyl 4-(2-pyridyldithio)-2-sulfobutanoate (sulfo-SPDB) linker-payload (17). Interestingly, most of these ADCs contain either monomethyl auristatin F (MMAF) or N2'-Deacetyl-N2'-(4-mercapto-4-methyl-1-oxopentyl)-maytansine (DM4), suggesting a relationship with the drug linker. However, albeit to a lower percentage, ocular toxicities have also been observed for ADCs with vcMMAE drug linkers (18). Prophylactic steroid eye drops are being used in several clinical trials as a potential mitigation and toxicity management strategy (3). Importantly, very little is known about the determinants of ocular toxicity or ways to design ADCs with lower propensity for this toxicity.

Agensys, Inc., Santa Monica, California.

Note: Supplementary data for this article are available at Cancer Research Online (http://cancerres.aacrjournals.org/).

Corresponding Author: Fernando Doñate, 1800 Stewart Street, Santa Monica, CA 90404. Phone: 424-280-5295; Fax: 424-280-5044; E-mail: fdonate@agensys.com

doi: 10.1158/0008-5472.CAN-17-3202

The cornea is composed of layers of epithelial cells in an avascular environment and a thick substratum. Corneal epithelial cells originate from stem cells in the vascularized limbal region [limbal stem cells (LSC); ref. 19]. LSCs migrate toward the central and outer region of the cornea while becoming more differentiated. It is estimated that the half-life of human corneal epithelium is 3 days, and it takes about 20 days in humans to fully replace this epithelium (19, 20).

AGS-16C3F is an ADC against ENPP3 (21) being developed for the treatment of metastatic renal cell carcinoma currently in a phase II study (ClinicalTrials.gov Identifier: NCT02639182). Two of the most common toxicities of AGS-16C3F are corneal toxicity and thrombocytopenia (8). Seeking to better understand the mechanism(s) of corneal toxicity for AGS-16C3F and other ADCs, *in vitro* assays using primary cells and a rabbit model were developed. The results suggested that AGS-16C3F is internalized into primary cells by macropinocytosis, and the charge and hydrophobicity of the ADC, in particular within the amino acid sequence, contribute to this process, resulting in off-target toxicities.

Materials and Methods

Cell lines and reagents

All cells were maintained according to vendors' protocol. Human primary corneal epithelial cells (HCEC) from Life Technologies (catalog no. C018-5C) were cultured in kertinocyte-SFM (catalog no. 17005-42), and HCEC cells from ATCC (catalog no. PCS-700-010) were cultured in corneal epithelial cell basal medium (catalog no. PCS-700-030) supplemented with corneal epithelial cell growth kit (catalog no. PCS-700-040). Human umbilical vein endothelial cells (HUVEC, catalog no. C-003-5C) and human dermal fibroblasts, adult (HDFa, catalog no. C-013-5C) were from Life Technologies. HUVECs were grown in Medium 200 supplemented with low serum growth supplement (LSGS, catalog no. S-003-10). HDFa cells were grown in Medium 106 supplemented with LSGS. KU812 cells were from ATCC (catalog no. CRL-2099) and were grown in RPMI1640 plus 10% FBS as described previously (21). Cell lines were passaged in our laboratory for fewer than 6 months after their resuscitation. Human cell lines were confirmed utilizing short tandem repeat profiling (Promega) and confirmed to be *Mycoplasma* negative (22). Reagents for human hematopoietic stem cells (HSC) and their differentiation to megakaryocytes were reported previously (5, 6). T-DM1 (Kadcyla; Genentech/Roche) was purchased (Myoderm).

Antibody and ADC generation

Mutations of the AGS-16C3F antibody variable region were generated by site-directed mutagenesis. Expression constructs encoding both the heavy and light chains of AGS-16C3 and mutants were stably transfected into Chinese hamster ovary (CHO) cells. Following purification, antibodies were conjugated to MMAF via the linker maleimidocaproyl (mc) and to MMAE via the cleavable drug linker maleimidocaproylvaline-citrulline-p-aminobenzyloxycarbonyl as described previously (5, 21). The anti-folate receptor-α (Rα), IMGN853 IgG1κ antibody was cloned, expressed, and purified from CHO cells, and conjugated to the drug linker DM4-SPDB (4.9 molar equivalents) in the presence of 25 mmol/L sodium borate pH 8.5 and 10% DMSO cosolvent for 1 hour at room temperature. The resulting conjugate was purified by PD10 desalting columns and eluted in 20 mmol/L histidine pH 5.2 containing 5% trehalose. The drug-to-antibody ratio (DAR) was determined by UV/VIS absorbance ratio of drug relative to antibody.

Peptide conjugation

The human IgG_2-based ADC, AGS-16C3F, formulated in 20 mmol/L histidine pH 5.2 containing 5% sucrose, was buffer exchanged to 20 mmol/L sodium succinate buffer pH 4.3 using PD10 desalting columns. The pH was adjusted to 9 using a sodium borate stock buffer, and an azido-PEG4-NHS ester bifunctional linker (Thermo Fisher Scientific, catalog no. 26130) was conjugated to the antibody lysine residues by incubating at room temperature for approximately 90 minutes. Unreacted linker was quenched with excess ethanolamine. The reaction mixtures were acidified by adding a glycine pH 3.0 stock buffer, and the resulting conjugates, with free azido groups, were purified using PD10 desalting columns and eluted into 20 mmol/L histidine pH 5.2 containing 5% trehalose. A CKKKKK or CEEEEE polypeptide (NeoBioLab) was conjugated via the free thiol of cysteine to a DBCO-maleimide bifunctional linker (Click Chemistry Tools, catalog no. A108-100) at pH 7.4 for 80 minutes at room temperature. The resulting constructs were then conjugated to the free azido groups installed on the AGS-16C3F in the previous step by incubating for approximately 24 hours at room temperature. Resulting conjugates were purified by PD10 desalting columns and eluted in either 20 mmol/L histidine pH 5.2 containing 5% trehalose or 20 mmol/L Tris pH 7.4 containing 5% trehalose for CKKKKK and CEEEEE conjugates, respectively. The polypeptide/antibody ratio for each conjugate was determined by calculating a weighted average of each detected conjugate peak by LC/MS.

Pegylation

AGS-16C3F was buffer exchanged into pH 5.2, 20 mmol/L succinate to a final concentration of 6.1 mg/mL. To this solution were added pH 9.0, 0.5 mol/L sodium borate buffer (50 mmol/L final) and 9 molar equivalents of mPEG8-NHS (Quanta BioDesign, catalog no. PN 10260) in DMSO (20 mmol/L), and then reacted for 1 hour at ambient temperature. The ADCs were purified by desalting column with 20 mmol/L histidine, 5% trehalose, and pH 5.2 buffer. The product was sterile filtered and stored at −80°C.

Macropinocytosis

HSCs (10^5 cells/well) were grown in 24-well plates overnight and then incubated with 1 mg/mL dextran-FITC (10,000 MW, Life Technologies) for 3 hours at 37°C or 4°C as control. Cells were detached with trypsin and neutralized with neutralization solution (Life Technologies, catalog no. R002100). Cells were then washed three times with FACS stain buffer (FBS, BD Pharmingen, catalog no. 554656) and analyzed by Attune acoustic focusing cytometer (Life Technologies). To test the effect of 5-(N-ethyl-N-isopropyl)amiloride (EIPA), indicated amount of EIPA was added to cell culture 30 minutes prior to dextran-FITC addition. Median fluorescence intensity ratio (MFIR) was derived from MFI values at 37°C normalized against those at 4°C.

Proliferation assays

HCECs (500 cells/well) and HUVECs (2,000 cells/well) in 100 μL were seeded in collagen-coated 96-well plates (Corning, catalog no. 354650), and HDFa (2,000 cells/well) and KU812

(2,500 cells/well) in 100 μL were grown in 96-well tissue culture plates (Corning assay plate, catalog no. 3903). After treatment with ADCs for 6 days, CellTiter-Glo (CTG) luminescence assay kit (Promega, catalog no. G7572) was used to measure the viability of the treated cells relative to control. CTG values were normalized against mock-treated cells at day 6 (% max proliferation), and GraphPad Prism 6 was used to generate IC_{50} values using a sigmoidal dose–response (variable slope). Assay plates contained technical triplicates for each drug concentration, and data presented are the mean of at least two independent determinations.

ANS assay

ADCs (2 mg/mL) were prepared in PBS, and 1:2 serial dilutions were made in a black-walled, 96-well plate (21, 23). Equal volume of 1,8-ANS (1-anilinonaphthalene-8-sulfonic acid, Thermo Fisher Scientific, catalog no. A47) was added and incubated for 30 minutes at room temperature. Fluorescence signal was measured (ex. 390 nm/em. 470 nm). Hydrophobicity index was the slope from the linear regression analysis.

Confocal microscopy

Cells were seeded on 8-well chamber slides (0.75×10^5 cells per well) and cultured for 48 hours prior to treatment and subsequent immunostaining. Cells were then incubated with AGS-16C3F with and without coincubation of 0.5 mg/mL Dextran-Texas Red (Molecular Probes; D18653) for 4 hours at 37°C. Inhibition of macropinocytosis was evaluated by treating cells with EIPA for 30 minutes prior to AGS-16C3F/Dextran-Texas Red incubation. After the incubation period, unbound antibody was washed off with PBS and cells were fixed in 4% paraformaldehyde for 20 minutes at room temperature. Cells were then permeabilized in PBS plus 0.1% Triton-X-100 for 15 minutes, and nonspecific labeling was blocked in PBS plus 10% normal goat serum. Cell surface–bound and internalized cytosolic AGS-16C3F was visualized by incubating cells with Alexa Fluor 488–labeled goat anti-human IgG (Thermo Fisher Scientific, catalog no. A-11013). Nuclei were visualized with TO-PRO-3 Iodide (Thermo Fisher Scientific, catalog no. T3605), and coverslips were mounted using ProLong Gold Antifade reagent (Thermo Fisher Scientific, catalog no. P36934) for imaging. High-resolution laser confocal image sections were acquired using a Leica TCS SP5 II (63x oil immersion objective; NA = 1.4) and were scanned sequentially to minimize fluorophore cross-talk and false-positive colocalization.

Animal studies and welfare

In vivo xenografted tumor models and pharmacodynamic studies were carried out as described before (21, 23). All experimental protocols were approved by Agensys' Institutional Animal Care and Use Committee. All procedures in the toxicology studies were in compliance with the Animal Welfare Act and Regulations (9 C.F.R. 3). Male Dutch Belted [Haz:(DB)SPF] rabbits weighing approximately 1.5 to 2.0 kg were used for ocular tolerability studies. Rabbits were acclimated for at least 6 days prior to first dose. All animals were housed in individual, suspended, stainless steel caging, were provided feed and water, and were maintained under environmental conditions in compliance with all animal welfare guidelines. Test articles were administered to groups of 3 to 4 rabbits intravenously via a marginal ear vein, followed by a saline flush once weekly for up to six doses (days 1, 8, 15, and 22). General health was assessed by weekly measurement of body weight and cage-side observations. Ocular tolerability was assessed by external examination—slit lamp biomicroscopy to examine the adnexa and anterior portion of each eye. In addition, the ocular fundus was examined using an indirect ophthalmoscope following dilation with a mydriatic agent. Corneal fluorescein staining was also performed to examine corneal damage. A fluorescein solution (approximately 1 mg/mL) was applied to the cornea by a cotton-tipped swab. At necropsy, eyes and other selected tissues were placed in fixative according to established procedures for IHC. All rabbit studies were performed by Covance Laboratories.

Statistical analysis

Statistical analysis was performed using unpaired *t* test method and the GraphPad Prism software. Statistical significance is reported as significant (**, $P < 0.05$). Statistical analysis of the tumor volume data for the last day before animal sacrifice was performed using the Kruskal–Wallis test. The implementation of the Kruskal–Wallis test was carried out using the parametric ANOVA F-test on the ranks of the data. Pairwise comparisons were made using the Tukey–Kramer method (two sided).

Results

AGS-16C3F has been shown to induce reversible ocular toxicity in patients, including corneal deposits, blurred vision, keratitis, and dry eye (8). Investigation of ENPP3 expression in human and cynomolgus monkey corneas by IHC showed no detectable signal (Supplementary Fig. S1). In contrast, no clinical ocular findings were noted in cynomolgus monkeys treated with AGS-16C3F at 6 mg/kg once weekly for four doses [highest doses tested and the no-observed-adverse-effect level (NOAEL)] or up to six doses, (Agensys; data on file). The only abnormality observed was a moderate and variable increase in the number of mitotic figures and apoptotic cells in the cornea of some of the treated animals after six doses (Agensys; data on file).

An *in vitro* system was developed to culture HCECs to investigate the determinants of ocular toxicity. HCECs are human corneal epithelial cells isolated from the limbal region (20), which express cytokeratin 15 (CK15) and p63α, but not ENPP3 (Supplementary Fig. S2A–S2C). As shown in Fig. 1A and Table 1, free MMAE, AGS-16C3F alone or in combination with an excess of naked antibody (AGS-16C3), and another anti-ENPP3–directed ADC (AGS-16M18F), were tested in the HCEC *in vitro* cytotoxicity assay. Free MMAE was used as a positive control for the anti-tubulin mechanism of action, as it is an auristatin similar to MMAF, but is nonpolar and thus freely crosses the cell membrane. As expected, it was potently cytotoxic with an IC_{50} of 0.4 ± 0.03 nmol/L. The HCECs were also highly sensitive to AGS-16C3F, with an IC_{50} of 5.6 ± 2.3 nmol/L. The activity of AGS-16C3F was not inhibited by the presence of an excess of AGS-16C3 in agreement with the lack of ENPP3 expression. In addition, AGS-16C3F was significantly more cytotoxic than AGS-16M18F (IC_{50} = 93.0 ± 27.1 nmol/L) despite both being directed against the same target, both possessing a similar DAR, both containing mcMMAF, and both being similarly cytotoxic against ENPP3-positive KU812 cells (AGS-16M18F IC_{50} = 0.09 ± 0.04 nmol/L vs. AGS-16C3F IC_{50} = 0.06 ± 0.02). These results suggested that

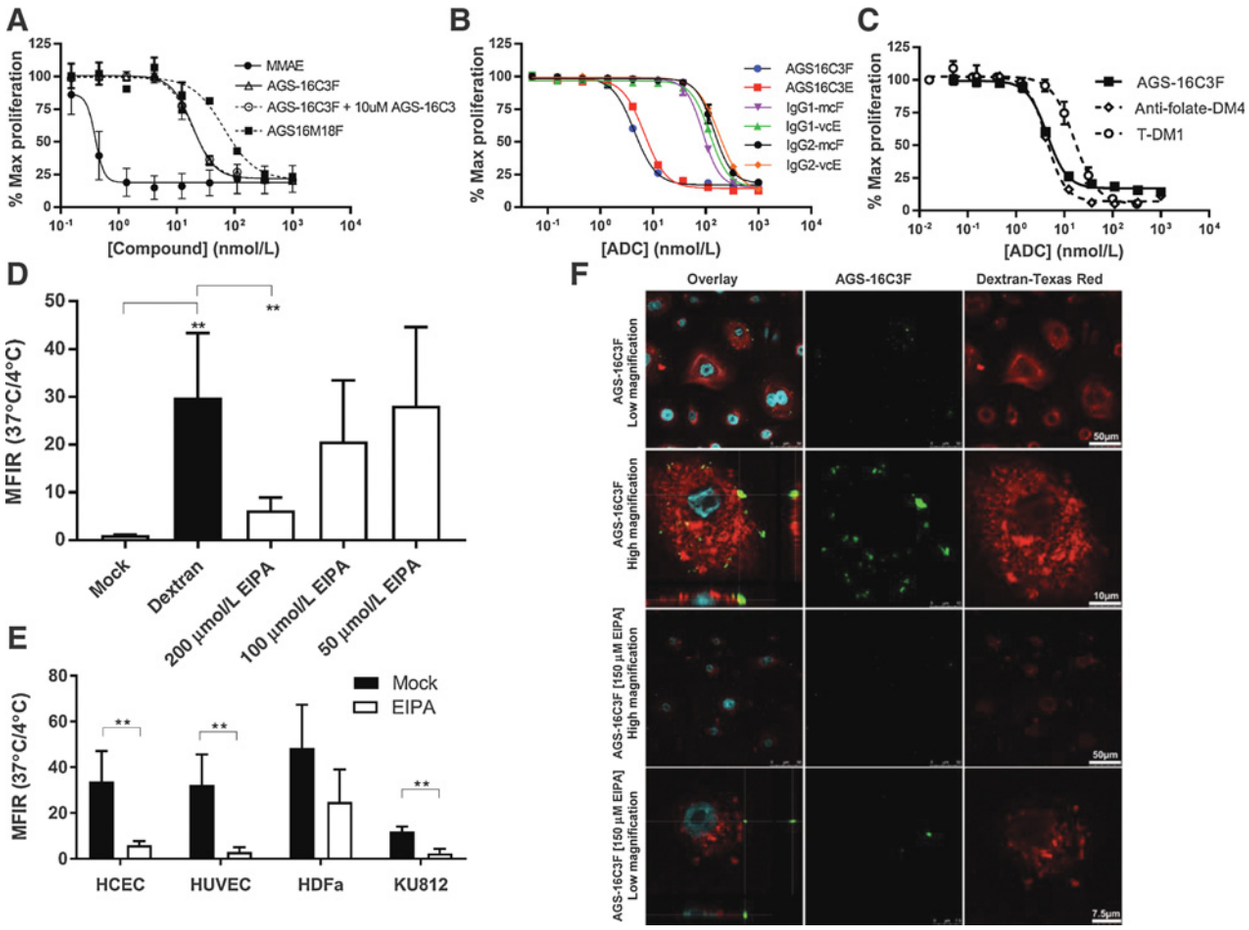

Figure 1.

AGS-16C3F is cytotoxic to HCECs and other primary cells after internalization by macropinocytosis. **A–C,** HCECs were grown for 6 days in the presence or absence of increasing concentrations of MMAE or ADCs, and cell viability was determined. The data shown are the mean of triplicates from a representative experiment of two to three independent experiments. **D,** HCECs were incubated with dextran-FITC (10,000 MW) alone or in the presence of EIPA (50–200 µmol/L) for 30 minutes at 4 and 37°C and analyzed by FACS. **E,** HCECs, HUVECs, HDFa, and KU812 cells were incubated with dextran-FITC (10,000 MW) alone or in the presence of EIPA (150 µmol/L) for 30 minutes at 4°C and 37°C and analyzed by FACS. The ratio of MIFR at 37°C over that at 4°C is shown in the *y*-axis. The data shown in **D** and **E** are the mean and SD of three independent experiments. **F,** Internalization of AGS-16C3F in HCEC. HCECs were incubated with AGS-16C3F in the absence of EIPA (first and second rows) and in the presence of EIPA (third and bottom row), and then fixed and stained as indicated. Samples were imaged using laser scanning confocal fluorescence microscopy. AGS-16C3F, green; Dextran-Texas Red, red; nuclei, blue. Left column shows the 3-channel overlay including single plane Z-stack cross-sections (left column, middle image) through horizontal plane (XY), sagittal plane (YZ), and coronal plane (XZ). Statistical significance, **, $P < 0.05$.

other anti-ENPP3 ADCs containing mcMMAF can be identified with lower ocular toxicity. ADCs directed against non-human proteins conjugated to vcMMAE or mcMMAF and, as IgG_1 or IgG_2, showed significantly lower cytotoxicity than AGS-16C3F (Fig. 1B; Table 1). AGS-16C3 conjugated to vcMMAE (AGS-16C3E) had similar cytotoxicity compared with AGS-16C3F, suggesting that the effect is independent of these two types of drug linkers. ADCs against olfactory receptor family 51 subfamily E member 1 (OR51E1; H3.1.4.1.2-mcF) and CD37 (AGS67E) targets for which mRNA levels were negligible by microarray in HCECs (Supplementary Fig. S3) were also tested (Table 1) and showed lower cytotoxicity compared with AGS-16C3F. The cytotoxicity of two lots of H3.1.4.1.2-mcF with different DARs of 3.3 and 4.7 was similar (Table 1). Two other ADCs, T-DM1 and anti-folate Rα-DM4 (Fig. 1C; Table 1) directed to targets for which ocular toxicities in patients have been reported (12, 14), were also tested in the HCEC cytotoxicity assay. Anti-folate-DM4 contains the same antibody as IMGN853, currently in phase III in ovarian cancer (14); however, the payload is SPDB-DM4 as opposed to the sulfo-SPDB-DM4 drug linker for IMGN853. The IC_{50} for two of these ADCs, the anti-folate-DM4 ($IC_{50} = 5.6 \pm 3.9$ nmol/L) and the T-DM1 ($IC_{50} = 14.4 \pm 3.8$ nmol/L) were similar to that of AGS-16C3F in agreement with the toxicity encountered in humans in those three programs. The expression in the cornea of the targets to which these ADCs are directed was not independently investigated as part of this study; however, HER-2 has been reported at low levels in the cornea (16), and this may be the cause of the cytotoxicity in HCEC, whereas FOLR1 is not expressed (2). Analysis of HCEC and human corneas confirmed positive levels of HER-2 as

Table 1. Characteristics of ADCs tested and IC_{50} in the HCEC assay

ADC	Target	Drug linker	IgG class	DAR	IC_{50} in HCEC assay (nmol/L)
MMAE	N/A	N/A	N/A	N/A	0.4 ± 0.03
AGS-16C3F	ENPP3	mcMMAF	IgG_2	4.2	5.6 ± 2.3
AGS-16C3E	ENPP3	vcMMAE	IgG_2	4.7	4.5 ± 2.9
AGS-16M18F	ENPP3	mcMMAF	IgG_1	4.3	93.0 ± 27.1
AGS67E	CD37	vcMMAE	IgG_2	3.9	65.8 ± 10.7
AGS67F	CD37	mcMMAF	IgG_2	3.6	86.4 ± 25.6
IgG_1-vcMMAE	HEWL	vcMMAE	IgG_1	3.7	106.9 (119.7, 94)
IgG_1-mcMMAF	HEWL	mcMMAF	IgG_1	3.5	87.1 ± 12.5
IgG_2-vcMMAE	HEWL	vcMMAE	IgG_2	4.2	171.5 ± 8.7
IgG_2-mcMMAF	HEWL	mcMMAF	IgG_2	4.7	136.6 ± 29.2
IgG_2-DM4	HEWL	SPDB-DM4	IgG_2	4.3	11.6 ± 1.7
H3.1.4.1.2-mcF	OR51E1	mcMMAF	IgG_1	3.3	126.7 ± 16.5
H3.1.4.1.2-mcF	OR51E1	mcMMAF	IgG_1	4.7	192.4 (94.9, 289.9)
H3.1.4.1.2-vcE	OR51E1	vcMMAE	IgG_1	3.4	67.2 ± 11
H3.12bc1.1-mcF	OR51E1	mcMMAF	IgG_2	3.4	97.1 (91.2, 103.1)
T-DM1	HER-2	SMCC-DM1	IgG_1	3.5	14.4 ± 3.8
Anti-FOLRα-DM4	FOLR1	SPDB-DM4	IgG_1	3.4	5.6 ± 3.9

NOTE: Mean and SD of $n = 3$ or mean and values of $n = 2$.

Abbreviations: N/A, not applicable; ENPP3, ectonucleotide pyrophosphatase/phosphodiesterase 3; HEWL, hen egg white lysozyme; SMCC-DM1, succinimidyl trans-4-(maleimidylmethyl)cyclohexane-1-carboxylate (SMCC) linked to DM1 (succinimidyl-trans-4-(maleimidylmethyl) cyclohexane-1-carboxylate); sulfo-SPDB-DM4, N-Succinimidyl 4-(2-pyridyldithio)-2-sulfobutanoate linker (sulfo-SPDB) linked to DM4 (N2′-Deacetyl-N2′-(4-mercapto-4-methyl-1-oxopentyl)-maytansine.

mRNA, whereas that for FOLR1 was negligible (Supplementary Fig. S3). The IgG_2 against OR51E1 conjugated to SPDB-DM4 had an IC_{50} of 11.6 nmol/L (Table 1), approximately 10-fold lower than when conjugated with mcMMAF. AGS-16C3F was also cytotoxic to other primary cells *in vitro*, such as adult dermal fibroblasts (IC_{50} = 43.8 ± 15 nmol/L, n = 5) and HUVEC (IC_{50} = 16 ± 11.3 nmol/L, n = 3), although neither of these cells bind AGS-16C3F as measured by flow cytometry (Supplementary Fig. S4A). Altogether, these data suggested that the biophysical properties of ADCs and not the drug linker, at least for vcMMAE and mcMMAF, the target or the IgG subtype were responsible for their cytotoxic activity against HCECs and other primary cells.

Our group has recently published results supporting that AGS-16C3F is cytotoxic to differentiating megakaryocytes by macropinocytosis-mediated internalization (6). To determine whether HCECs and other primary cells had the ability to readily undergo macropinocytosis, the internalization of the fluorescence probe dextran-fluorophore, commonly used to measure micropinocytosis (6), was tested (Fig. 1D–F) and was shown to be incorporated (Fig. 1D). Internalization by macropinocytosis can be blocked by EIPA (6, 24), an inhibitor of Na^+/H^+ exchange. EIPA inhibited internalization of dextran-FITC into HCEC in a concentration-dependent manner (Fig. 1D). HUVECs, fibroblasts, as well as HCECs also internalized the fluorescent dye to higher levels than the ENPP3-positive tumor cell line KU812 (Fig. 1E). EIPA inhibited internalization of the dextran-fluorophore by more than 80% in HCECs and HUVECs in agreement with macropinocytosis mediating internalization. The inhibition was lower for fibroblasts, suggesting that the dextran internalization occurs by macropinocytosis and other unknown mechanism(s) in these cells. In addition, internalization of AGS-16C3F into HCEC was observed by confocal microscopy. As shown in Fig. 1F, AGS-16C3F was internalized by HCECs and colocalized with dextran-Texas Red. Furthermore, the internalization of both was partially inhibited by EIPA cotreatment, consistent with data in Fig. 1E, suggesting macropinocytosis-mediated internalization. EIPA was toxic to HCEC, precluding testing at higher concentrations or in the 6-day HCEC proliferation assay. These data suggest that AGS-16C3F is internalized in ENPP3-negative primary cells by macropinocytosis.

The mechanism of internalization of macromolecules by macropinocytosis is poorly understood. It has been proposed that it is mediated by nonspecific interactions with the normally negatively charged membrane determined by hydrophobicity and/or the presence of positive charges in the macromolecule (25, 26). Thus, the cytotoxicity of AGS-16C3F against HCECs may be due to the presence of exposed hydrophobic residues or positively charged amino acids. Three different experimental approaches were undertaken to investigate these hypotheses: attachment of charged polypeptides or polyethylene glycol (PEG) moieties to AGS-16C3F, and mutation of surface-charged residues in AGS-16C3F.

To test the potential role of negative or positive charges in the AGS-16C3F macropinocytosis-mediated internalization in HCEC, polyglutamate or polylysine peptides (PLE or PLK, respectively) of different sizes were conjugated through lysines to AGS-16C3F and tested in the HCEC assay (Fig. 2A; Supplementary Table S1). Interestingly, AGS-16C3F conjugated to negatively charged PLE was less cytotoxic, whereas AGS-16C3F conjugated to the positively charged PLK was more cytotoxic to HCECs than AGS-16C3F (Fig. 2A). PLK conjugation to AGS-16C3F also significantly increased ADC binding to HCECs (3.9- to 33-fold), as measured by flow cytometry, but not PLE conjugation (Supplementary Table S1). Peptide conjugation [up to peptide-to-antibody ratio (PAR) of 3] had little effect on affinity to ENPP3 protein and cytotoxicity to tumor cells *in vitro*, whereas it had a significant effect on ADC binding and cytotoxicity to HCECs (Supplementary Table S1). AGS-16C3F and AGS-16C3F-PLK were internalized by HCEC, but AGS-16C3F-PLE internalization was not detected by confocal microscopy (Fig. 2B). Similar to the effects on HCECs, peptide conjugation to AGS-16C3F modulated the cytotoxic activity against other primary cells such as HUVECs (Fig. 2C) and differentiating megakaryocytes (Fig. 2D). The IC_{50} in two fibroblast cytotoxic activity studies for AGS-16C3F-PLE, AGS-16C3F, and AGS-16C3F-PLK were 95.0 nmol/L, 66.6 nmol/L, and 69.7 nmol/L, respectively, representing a modest

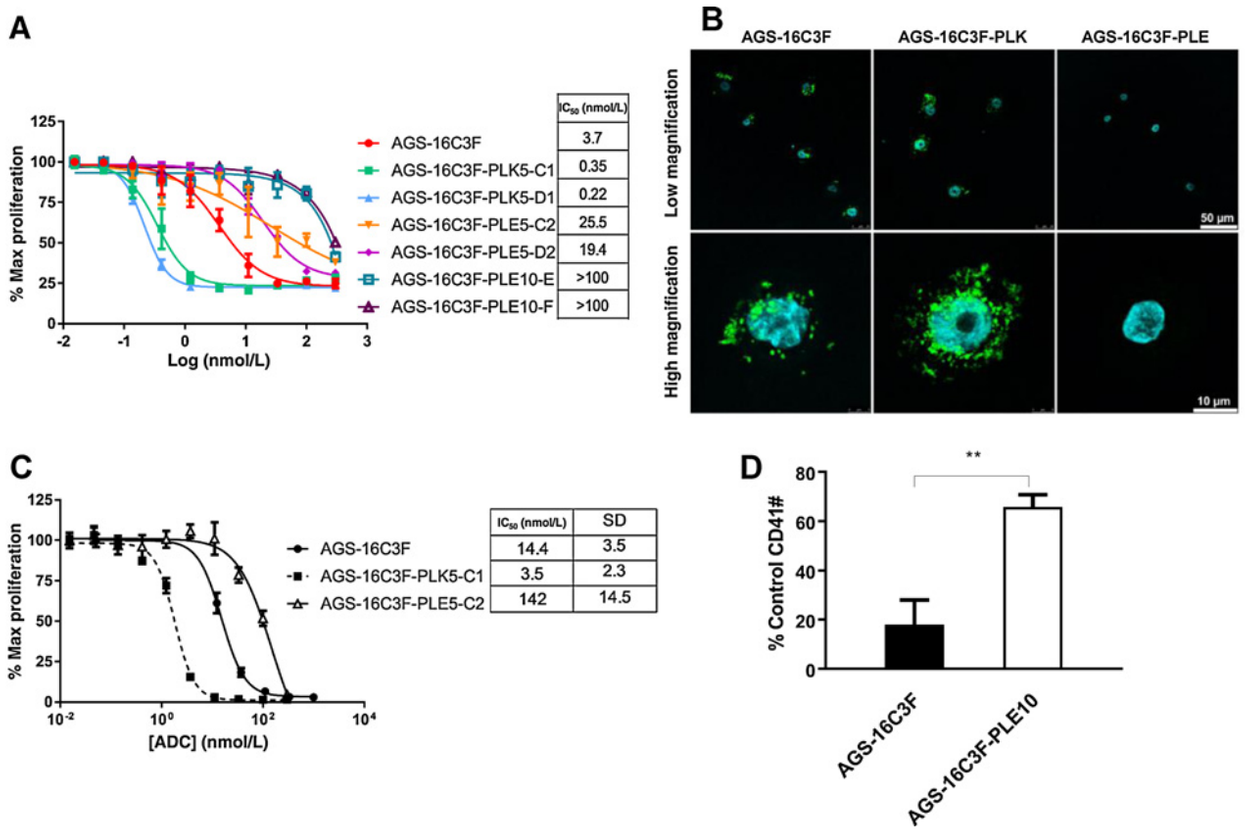

Figure 2.

Attachment of poly-K or poly-E peptides to AGS-16C3F enhances or inhibits internalization and subsequent cytotoxicity. **A,** HCECs were grown for 6 days in the presence or absence of increasing concentrations of AGS-16C3F conjugated to polylysines (AGS-16C3F-PLK) or polyglutamate (AGS-16C3F-PLE), and cell viability was determined. The inset table shows the IC_{50} for each ADC tested. Data are from a representative experiment of two to three independent experiments. **B,** Internalization of AGS-16C3F, AGS-16C3F-PLK, and AGS-16C3F-PLE in HCECs. HCECs were incubated with ADCs (green), and then fixed and stained as indicated. Samples were imaged using laser scanning confocal fluorescence microscopy. **C,** HUVECs were grown for 6 days in the presence or absence of increasing concentrations of ADCs, and cell viability was determined. The inset table shows the IC_{50} for each ADC tested. The data shown are the mean and SD of three independent experiments. **D,** After 3-day expansion, differentiating HSCs were grown in MK differentiation medium for 1 day and were treated for 6 days with either 100 nmol/L of AGS-16C3F or AGS-16C3F-PLE10. $CD41^+$ cells were measured with FACS, and the number of $CD41^+$ cells was normalized against mock-treated samples. The data shown are the mean and SD of three independent experiments. Statistical significance, **, $P < 0.05$.

reduction of cytotoxicity for the PLE-conjugated AGS-16C3F. Altogether, the data suggested that electrostatic interactions are contributing to macropinocytosis-mediated nontarget toxicities independent of cell type. Modifications in the charge of the ADC reduced the toxicity against HCECs and other primary cells while preserving the *in vitro* antitumor activity of the modified ADC. It is possible that the hydrophobicity of AGS-16C3F was also decreased by attaching charged residues inducing a decrease in macropinocytosis; however, the PLK-modified AGS-16C3F was more cytotoxic despite this possible decrease in hydrophobicity.

The degree of hydrophobicity for AGS-16C3F and other ADCs was determined using 8-anilinonaphthalene sulfonate (ANS), a hydrophobic probe whose fluorescence increases upon binding to hydrophobic areas (27). As shown in Fig. 3A, AGS-16C3F was more hydrophobic than an IgG_2-mcMMAF ADC, H3.1.4.1.2-mcF, and T-DM1. The higher degree of hydrophobicity of AGS-16C3F compared with T-DM1 can also be appreciated in a space-filled model of one of the CDR regions of AGS-16C3 compared with trastuzumab (Fig. 3B). A common method to decrease hydrophobicity of macromolecules is by attaching polymers of PEG (28–30). Thus, AGS-16C3F was modified through exposed lysines with PEGs, of different lengths and characterized for hydrophobicity index (ANS assay), binding to ENPP3 in cells and cytotoxicity in the HCEC and KU812 assays (Supplementary Table S2). All of the PEGylated AGS-16C3F derivatives showed decreased hydrophobicity from that of AGS-16C3F but retained their affinity for ENPP3 and *in vitro* cytotoxicity toward KU812 cells (Supplementary Table S2). Importantly, the PEGylated derivatives had reduced toxicity against HCEC. On the basis of these data, AGS-16C3F-mPEG8-9E was chosen for further studies. This variant internalized into HCECs to a lesser degree than AGS-16C3F, as shown by confocal microscopy (Fig. 3C), in agreement with the lower cytotoxicity against those cells. AGS-16C3F-mPEG8-9E was also less cytotoxic to differentiating megakaryocytes (Fig. 3D), HUVECs, and fibroblasts than AGS-16C3F (Fig. 3E). These data suggest that modulation of the hydrophobicity of AGS-16C3F by PEGylation reduces the cytotoxicity against HCEC and other primary cell types while preserving their target-dependent antitumor activity *in vitro*.

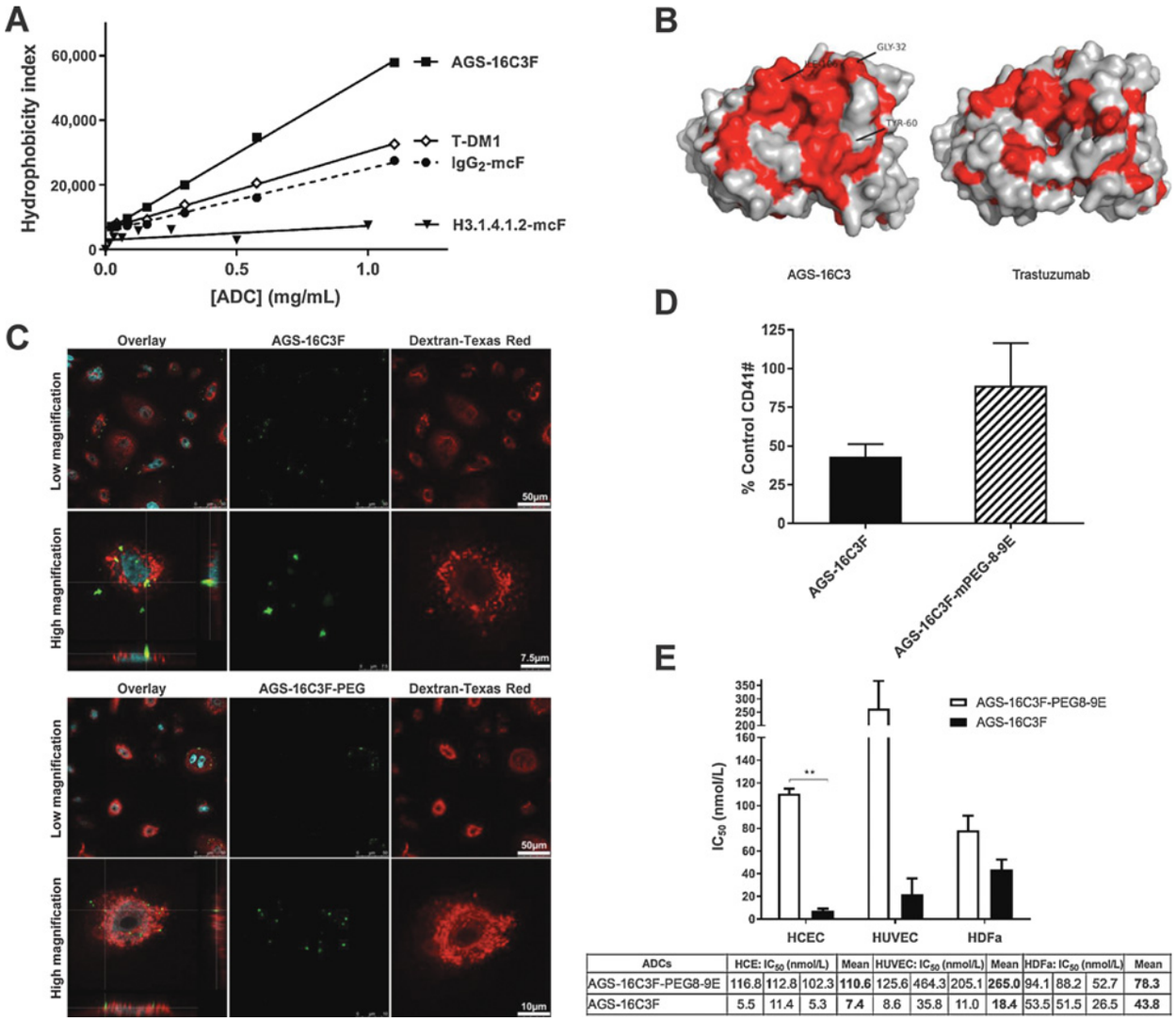

ADCs	HCE: IC_{50} (nmol/L)			Mean	HUVEC: IC_{50} (nmol/L)			Mean	HDFa: IC_{50} (nmol/L)			Mean
AGS-16C3F-PEG8-9E	116.8	112.8	102.3	**110.6**	125.6	464.3	205.1	**265.0**	94.1	88.2	52.7	**78.3**
AGS-16C3F	5.5	11.4	5.3	**7.4**	8.6	35.8	11.0	**18.4**	53.5	51.5	26.5	**43.8**

Figure 3.

AGS-16C3 antibody and ADC are hydrophobic. Decreasing hydrophobicity by attaching poly-PEG molecules to AGS-16C3F attenuates toxicity against HCECs and other primary cells. **A,** Different concentrations of ADCs were incubated with ANS for 30 minutes, and fluorescence intensity is shown. Data are from a representative experiment of two to three independent experiments. **B,** Top view of space-filling models showing a hydrophobic patch in a CDR region of AGS-16C3 compared with that of trastuzumab. Hydrophopbic residues are shown in red. **C,** Internalization of ADCs in HCECs. HCECs were incubated with ADCs, and then fixed and stained as indicated. Samples were imaged using laser scanning confocal fluorescence microscopy. ADCs, green; Dextran-Texas Red, red; nuclei, blue. Left column shows the 3-channel overlay, including single-plane, Z-stack cross-sections (second and fourth row) through horizontal plane (XY), sagittal plane (YZ), and coronal plane (XZ). **D,** Differentiating megakaryocytes were grown as indicated in the presence or absence of ADC, and total $CD41^+$ cells were measured by FACS and normalized against mock-treated samples. **E,** HCECs, HUVECs, and HDFa were grown for 6 days in the presence or absence of increasing concentrations of ADCs, and cell viability was determined. The data shown are the mean and SD of three independent experiments. Statistical significance, **, $P < 0.05$.

A more feasible approach to improve the therapeutic index (TI) of AGS-16C3F than the strategies described above is to mutate the sequence of the antibody, aiming to increase the number of negatively charged amino acids. Surface positively charged amino acids outside the CDR were selected (Fig. 4A; ref. 31). Furthermore, the sequence of AGS-16C3F and of other antibodies, which as ADCs induced low cytotoxicity in the HCEC assay, were compared (Fig. 4B). Positions in which there was a negative/neutral charged residue in any of the other less toxic ADCs, but not at AGS-16C3F, were also considered for mutagenesis. The selected residues were, at heavy chain: K13, Q16, K45, K83, and A90; and at light chain: K16, K18, K45, and S60. Some of the residues (heavy chain, Q16E and light chain, R18S and K45E) had been mutated in previous publications aiming to decrease clearance of the antibodies (31).

The nine AGS-16C3 mutants were produced, purified, conjugated to mcMMAF, and tested in the HCEC and KU812 assays (Supplementary Table S3). The AGS-16C3F(A90E) mutant presented with problems of reproducibility that precluded further

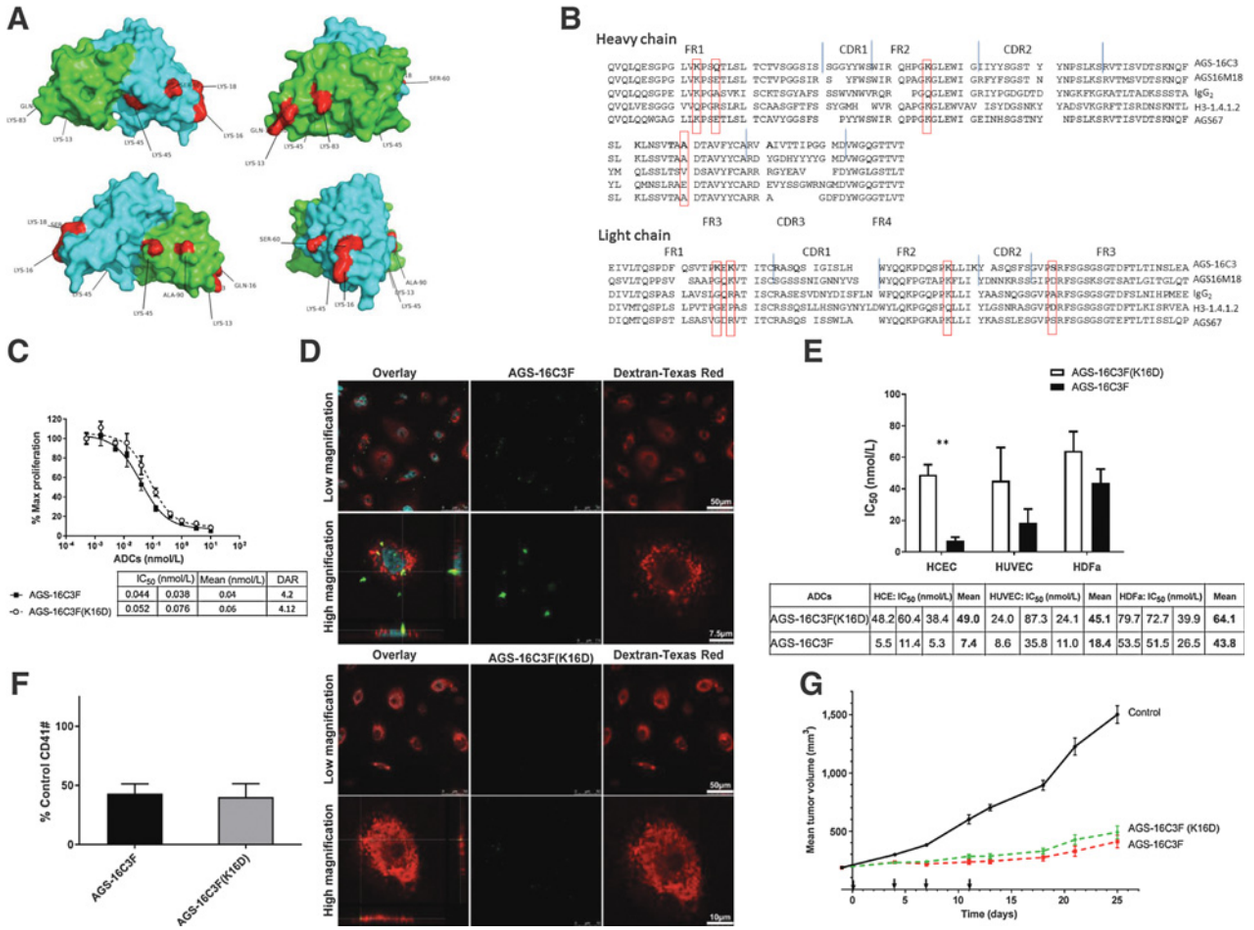

Figure 4.

Mutating positively charged residues in the surface of AGS-16C3F decreases cytotoxicity against HCEC and other primary cells while preserving the antitumor activity. **A,** Four views, rotated 90° of space-filling models of AGS-16C3F showing surface location of residues heavy chain: K13, Q16, K45, K83 and A90; light chain: K16, K18, K45 and S60. **B,** Sequence alignments. **C,** KU812 cells were grown for 6 days in the presence or absence of increasing concentrations of ADCs, and cell viability was determined. **D,** Internalization of AGS-16C3F and AGS-16C3F(K16D) in HCEC. HCECs were incubated with ADCs, then fixed and stained as indicated. Samples were imaged using laser scanning confocal fluorescence microscopy. ADCs, green; Dextran-Texas Red, red; nuclei, blue. Left column shows the 3-channel overlay including single-plane, Z-stack cross-sections (second and fourth row) through horizontal plane (XY), sagittal plane (YZ), and coronal plane (XZ). **E,** HCECs, HUVECs, and HDFa were grown for 6 days in the presence or absence of increasing concentrations of ADCs, and cell viability was determined The inset table shows the IC_{50} for each ADC tested. **F,** Differentiating megakaryocytes were grown as indicated in the presence or absence of ADC and total $CD41^+$ cells were measured by FACS and normalized against mock-treated sample. The data shown are the mean of triplicates from a representative experiment of three independent experiments. **G,** Mice ($n = 8$) bearing 200–250 mm^3 UG-K3 RCC xenografted tumors were treated with AGS-16C3F or AGS-16C3F(K16D) at 0.25 mg/kg by i.v. injection on days 0, 4, 7, and 11 (arrows). Data show mean ± SEM tumor volume for each group. Statistical significance, **, $P < 0.05$.

characterization. The DAR of these ADCs varied (2.9–4.2 vs. 4.0 for AGS-16C3F), as the conjugation was not optimized for each mutant. To correct for the DAR variability, the ratios of IC_{50} to both HCEC and KU812 cytotoxicity assays were normalized to that ratio for AGS-16C3F. The results showed that three mutants had an improved TI. For proof-of-concept analysis, AGS-16C3F(K16D) was chosen, because it preserved the *in vitro* antitumor activity against KU182 ($IC_{50} = 0.06$ nmol/L vs. 0.04; Fig. 4C), had a significant improvement in the cytotoxicity against HCECs ($IC_{50} = 23.7$ nmol/L vs. 6.3 nmol/L; Supplementary Table S3), and had a similar DAR than AGS-16C3F (4.2 vs. 4.0; Supplementary Table S3). Furthermore, AGS-16C3 contains a lysine in that position, whereas the other antibodies tested contained glycine (Fig. 4B). AGS-16C3F(K16D) appeared to internalize to a lesser degree into HCECs than AGS-16C3F, as detected by confocal microscopy (Fig. 4D), and was also less cytotoxic to HUVECs and fibroblasts than AGS-16C3F (Fig. 4E); however, it was equally cytotoxic to differentiating megakaryocytes (Fig. 4F). The *in vivo* antitumor activity of AGS-16C3F(K16D) mutant was tested in a patient-derived renal cell carcinoma xenograft model, UG-K3, in which the efficacy of AGS-16C3F had been previously established (21). As shown in Fig. 4G, the AGS-16C3F(K16D) mutant had comparable antitumor activity [tumor growth inhibition (TGI) = 76.9%; ref. 23] to AGS-16C3F (TGI = 83.0%). Because similar mutations have been shown to extend the half-life of antibodies (31), the mouse PK of AGS-16C3F(K16D) and wild-type

Table 2. Ocular toxicity of rabbits treated with AGS-16C3F and controls

Treatment	Study	ADC (mg/kg)	Number of animals	Ocular symptom (day)	Unscheduled death (day)
Vehicle	493[a]	N/A	3	$n = 0$[b]	$n = 0$
AGS-16C3F	493	5	3	$n = 0$	$n = 0$
AGS-16C3F	493	10	3	$n = 2$, (22) $n = 1$, (25)	$n = 2$, (22)[c]
AGS-16C3F	493	15	3	$n = 2$, (18) $n = 1$, (25)	$n = 1$, (39)[d]
Vehicle	275[e]	N/A	3	$n = 0$	$n = 0$
AGS-16C3F	275	15	3	$n = 2$, (21) $n = 1$, (26)	$n = 0$
H3.1.4.1.2-mcF	275	15	3	$n = 0$	$n = 0$
Vehicle	867[f]	N/A	4	$n = 0$	$n = 0$
AGS-16C3F	867	15	4	$n = 2$, (18)[g] $n = 1$, (25)	$n = 1$, (22)[h]
AGS-16C3F(K16D)	867	15	4	$n = 4$, (25)	$n = 0$

Abbreviations: N/A, not applicable; n, number of rabbits.

[a]Ophthalmologic examinations were carried out pre-dose and once a week. An unscheduled examination took place on day 22.

[b]Minor fluorescein staining in one animal with no visible lesions on day 18.

[c]Rabbits were euthanized due to severe ophthalmologic findings.

[d]Rabbit found dead during recovery from anesthesia, possibly also related to lack of weight gain.

[e]Ophthalmologic examinations were carried out pre-dose and on days 12, 22, and 26.

[f]Ophthalmologic examinations were carried out on days 12, 18, and 25.

[g]To manage clinical observations, a rabbit was given flunixin meglumine (2 mg/kg), an anti-inflammatory and antipyretic agent, starting at day 16 and continuing to day 22, when it was euthanized. A second rabbit in this group was also similarly treated on day 17.

[h]Rabbit was euthanized due to severe ophthalmologic findings.

AGS-16C3F were compared, but exposures were shown to be similar: AUC_{last} of 777 versus 573 μg/day/mL, respectively (Supplementary Table S4). These data suggest that AGS-16C3F(K16D) containing a single mutation in the variable region of the antibody can reduce off-target toxicity on normal cells without affecting on-target cytotoxicity against tumor cells.

As discussed above, cynomolgus monkeys did not represent a sensitive model for AGS-16C3F–induced ocular toxicity, as reported in humans. Rabbits are commonly used to test possible drug-mediated eye toxicities (32) and were chosen to investigate the ocular toxicity of AGS-16C3F and other ADCs. *In vitro* cultured rabbit corneal epithelial cells did not bind AGS-16C3F, as determined by flow cytometry (Supplementary Fig. S4B), suggesting either a lack of expression of ENPP3 or no cross-reactivity with the ADC.

Three ocular studies testing AGS-16C3F and other ADCs were carried out in rabbits with similar results (Table 2). The first study was a dose titration (5, 10, and 15 mg/kg once weekly × 6) of AGS-16C3F (DAR = 4.1), which determined that a 5-mg/kg dose was safe, but 10- and 15-mg/kg doses induced toxicities. Rabbits dosed at 15 mg/kg once weekly experienced clinical toxicities in the eyes on day 18 posttreatment, including conjunctival hyperemia, perilimbal corneal haze, corneal edema, and ciliary flush (Fig. 5A; Table 2). Likewise, the 10-mg/kg once-weekly dose caused ophthalmologic toxicities leading to the euthanasia of two rabbits on day 22 (Table 2). In the remaining animals at both doses, the ocular findings diminished over time, such as that by week 6, and only a minor perilimbal corneal haze persisted. Thus, the toxicities were considered largely reversible, similar to the findings in humans (8). Noticeably, the AGS-16C3F (15 mg/kg)–treated rabbits had lower body weight gain (0.6% ± 3.9%) compared with vehicle-treated rabbits (9.5% ± 0.5%) over the dosing period (day 36), suggestive of systemic toxicity (Supplementary Table S5). This was in agreement with the low food intake and low feces output observed for that group. The next two studies were carried out at 15-mg/kg once-weekly × 4 dosing. Remarkably, corneal microcysts, similar to what has been seen in humans, were detected in of one of the rabbits treated with AGS-16C3F (Fig. 5A). Histologic examination of the eyes from AGS-16C3F–treated rabbits at terminal necropsy revealed variable cellular inflammation in the limbus in animals given a 15-mg/kg/dose of AGS-16C3F (Fig. 5B). AGS-16C3F also induced moderate hypercellularity in the marrow (Fig. 5C). Contrary to the toxicity observed for AGS-16C3F, another mcMMAF containing ADC (H3.1.4.1.2-mcF, DAR = 3.92), with an IC_{50} of 100 nmol/L in the HCEC assay, did not present with ocular toxicities after dosing at 15 mg/kg once weekly × 4 (Table 2). Furthermore, the body weight gain was similar to that of treated controls (Supplementary Table S5), and the bone marrow was slightly hypercellular, but less than for the AGS-16C3F–treated group (Fig. 5C). These results suggest that the sequence of the antibody greatly influences target-independent toxicities.

The effects of AGS-16C3F(K16D) (DAR = 4.04) in the rabbit model were also tested. The ocular effects induced by treatment with AGS-16C3F(K16D), although similar to those of AGS-16C3F (Table 2), occurred at day 25 versus day 18 for AGS-16C3F and were less severe. For instance, two of the animals dosed with AGS-16C3F needed to be treated with anti-inflammatory drugs to alleviate ocular toxicities, and one of them was euthanized on day 22, whereas none were for the AGS-16C3F(K16D)–treated group (Table 2). This improvement in the toxicity profile for AGS-16C3F(K16D) was consistent with the results from the HCEC assay, which showed an approximately 4-fold increase in IC_{50}. Bone marrow collected at the end of study was noted on histopathology examination to have similar hypercellularity as that of rabbits treated with AGS-16C3F. A pharmacokinetic study in rabbits showed no major differences in exposure for AGS-16C3F and AGS-16C3F(K16D) (Supplementary Table S4). Altogether, these results suggest that modifications in AGS-16C3F can alleviate toxicities, as reflected in delayed and less severe ocular toxicity for AGS-16C3F(K16D).

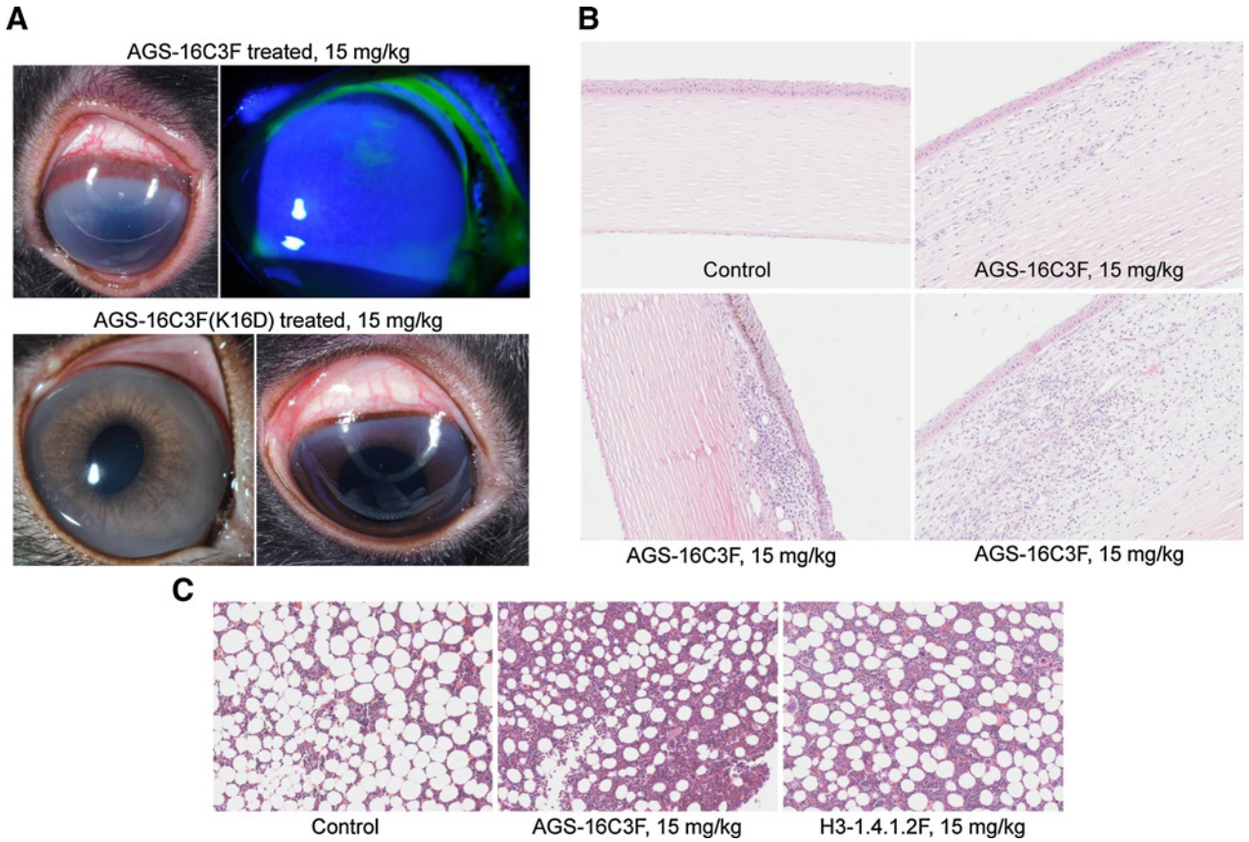

Figure 5.

AGS-16C3F induces ocular toxicities and hypercellularity in the bone marrow of rabbits. **A,** Images of the eyes of rabbits treated with ADCs showing corneal edema (top left); fluorescein staining was retained in a multifocal punctate pattern peripherally, a finding which was consistent with the presence of corneal microcysts (top right); and varying degrees of corneal edema (bottom two panels). **B,** Images of hematoxylin and eosin staining of corneas from AGS-16C3F (15 mg/kg, once weekly x 4) or vehicle control (top left)–treated rabbits showing various levels of inflammation: normal cornea (top left), slight inflammation in the subepithelial compartment (top right), notable inflammation in the limbal region (bottom left), and significant generalized inflammation throughout the subepithelial layer (bottom right). **C,** Images of hematoxylin and eosin staining of bone marrows of rabbits treated with ADCs or vehicle control.

Discussion

The data presented here support that AGS-16C3F is internalized in primary cells such as corneal epithelial cells, fibroblasts, and HUVECs by macropinocytosis, causing inhibition of cell proliferation. These results are an extension of our recent work suggesting that AGS-16C3F–mediated thrombocytopenia was caused by macropinocytosis-dependent internalization into differentiating megakaryocytes (6). This receptor-independent internalization results in off-target toxicities in the cornea and in other organs. Remarkably, modifications of the charges and/or hydrophobicity of AGS-16C3F modulated the cytotoxicity to primary cells. Furthermore, although the conclusions in this manuscript are mostly based on the results using AGS-16C3F, similar results and conclusions were obtained in a more limited number of experiments with other ADCs containing different drug linkers.

Our results support that macropinocytosis-mediated internalization is dependent on the presence of positive charges and/or the hydrophobicity of the antibody sequence and ADC. The cytotoxicity of AGS-16C3F was independent of antibody isotype or the type of drug linker, mcMMAF or vcMMAE, and was mainly dictated by the antibody sequence. For instance, AGS-16C3F(K16D) had lower cytotoxicity against primary cells and a better toxicity profile in the rabbit model than AGS-16C3F. Importantly, an mcMMAF containing ADC (H3.1.4.1.2-mcF) had an IC_{50} of 100 nmol/L in the HCEC assay, and the corresponding antibody of this ADC was less hydrophobic than AGS-16C3F (Fig. 3A). In addition, it contains seven favorable amino acids among the nine critical positions identified for AGS-16C3F (K13Q, K83Q, A90E, K16G, K18P, K45Q, and S60D; Fig. 4B). This ADC also had a favorable toxicity profile in the rabbit model at 15 mg/kg, whereas AGS-16C3F induced ocular toxicity at just 10 mg/kg. However, the pharmacokinetics of H3.1.4.1.2-mcF in rabbits was not determined, and these conclusions are only tentative. Decreasing the hydrophobicity of AGS-16C3F by PEGylation lowered the cytotoxicity to primary cells. These results are in agreement with previously published data showing that adding PEG moieties in the linker of ADCs with a DAR of 8 decreased the uptake in the liver by Kupffer cells by presumably ameliorating the hydrophobicity of these high-DAR species (29). Our results suggest that this uptake is also mediated by macropinocytosis. All of these

suggest that a lower hydrophobicity and/or the presence of neutral or negatively charged residues in some key exposed regions influence the cytotoxicity of ADCs against primary cells.

Interestingly, both, an anti-CDH6 sulfo-SPDB-DM4 as well as an IgG_1 sulfo-SPDB-DM4 control induced corneal toxicities in cynomolgus monkeys, suggesting that the toxicity was caused by the linker-payload and not by engagement of the target in the cornea or by the attributes of the antibody (17). Consistent with this conclusion, an IgG_2 antibody conjugated to a similar drug-linker, SPDB-DM4, had an IC_{50} of 11.6 nmol/L in the HCEC proliferation assay, whereas when conjugated to mcMMAF, it was 136.6 nmol/L, approximately 10-fold less cytotoxic. Many DM4 containing ADCs induce ocular toxicities in patients (2, 3, 7). This may represent an example in which the type of drug-linker, and not the sequence of the antibody, influences target independent toxicities by affecting the charge and/or hydrophobicity facilitating macropinocytosis-mediated internalization, or by other unknown mechanisms.

Regarding approaches to improve the TI of ADCs and of AGS-16C3F in particular, mutations in the sequence, such as those explored here (K16D), are feasible and provide an improvement in preclinical models. It is likely that other mutations and/or multiple mutations could further improve the TI of AGS-16C3F. Other modifications such as conjugation of negatively charged polymers or polyPEG molecules may also improve the TI of ADCs *in vivo* by decreasing macropinocytosis. Alternatively, ADCs may be screened in the HCEC assay as a surrogate for receptor-independent toxicity to identify those with the lowest cytotoxicity. AGS-16M18F is an example of an ADC against ENPP3 with a better profile than AGS-16C3F in the HCEC assay. Ultimately, pharmacologic inhibition of the process of macropinocytosis may be needed.

An open question is the significance of the rabbit model to the corneal toxicity of AGS-16C3F in humans. In support of being an appropriate model, rabbits had similar symptoms to those seen in humans with LSC deficiency (19), which is characterized by a loss or deficiency of stem cells and manifests as epithelial defects, chronic inflammation, keratitis, vascularization, and fibrosis. Some of these are similar to the findings observed after AGS-16C3F treatment in humans and in agreement with the results from an anti-5T4 mcMMAF ADC (PF-06263507) phase I study in which a patient was reported to have grade 1 LSC deficiency (15). We propose that ADCs reach the cornea through the vascularized area of the limbus, where they may be internalized by progenitor cells. As this a reversible toxicity, it seems unlikely that stem cells are affected. The distressed progenitor cells migrate radially and outward, where they may eventually die preventing the proper renewal of the corneal epithelium and causing the deposits sometimes observed in humans. Finally, steroid eye drops are being used prophylactically in clinical trials of several ADCs based on incidental findings of an improved toxicity profile in patients (3). Our results in the rabbit model offer evidence to explain the possible benefits of steroids as anti-inflammatory agents by preventing or decreasing the immune cell infiltration observed in the cornea of treated rabbits. Neutrophils present in these infiltrates may facilitate the release of MMAE from vcMMAE containing ADCs by secreting proteases (5). Importantly for the validation of these assays, there is consistency with regard to the data for AGS-16C3F on corneal cells from the *in vitro* HCEC assay, to the results in rabbits and to a lesser degree in monkeys, and finally humans. The full validation of these models awaits testing in humans of modified, improved versions of AGS-16C3F.

AGS-16C3F also induced other changes/toxicities in the rabbit such as hypercellularity in the bone marrow and insufficient weight gain. These results in the rabbit, together with the *in vitro* results using primary cells, suggest that receptor-independent toxicities to mcMMAF ADCs and possibly other ADCs share a common mechanism of action of internalization by macropinocytosis.

In conclusion, the work presented here suggests that macropinocytosis contributes to receptor-mediated internalization of ADCs and associated off-target toxicities. We proposed *in vitro* and *in vivo* assays to quantitate these toxicities and showed that some of the determinants of those toxicities are local charges and overall hydrophobicity of the antibody/ADC. This work may be applied to guide the design of ADCs with a significantly improved TI.

Disclosure of Potential Conflicts of Interest

All authors were employees of Agensys, Inc. during the period of the study.

Authors' Contributions

Conception and design: H. Zhao, J. Atkinson, Z. Zeng, J.W. Ou, P.M. Challita-Eid, S. Karki, D.R. Stover, F. Doñate

Development of methodology: H. Zhao, J. Atkinson, Z. Zeng, J.W. Ou, K. Morrison, P.M. Challita-Eid, S. Karki, J. Snyder, S.-J. Moon, B.A. Mendelsohn, F. Doñate

Acquisition of data (provided animals, acquired and managed patients, provided facilities, etc.): J. Atkinson, Z. Zeng, J.W. Ou, J. Nater, P. Yang, K. Morrison, J. Coleman, P.M. Challita-Eid, H. Aviña, R.S. Hubert, L. Capo, B.A. Mendelsohn, F. Doñate

Analysis and interpretation of data (e.g., statistical analysis, biostatistics, computational analysis): H. Zhao, J. Atkinson, S. Gulesserian, Z. Zeng, J.W. Ou, K. Morrison, J. Coleman, S. Karki, J. Snyder, R. Luethy, B.A. Mendelsohn, D.R. Stover, F. Doñate

Writing, review, and/or revision of the manuscript: H. Zhao, J. Atkinson, S. Gulesserian, J. Nater, J.W. Ou, P. Yang, K. Morrison, P.M. Challita-Eid, S. Karki, H. Aviña, D.R. Stover, F. Doñate

Administrative, technical, or material support (i.e., reporting or organizing data, constructing databases): D.R. Stover

Study supervision: H. Zhao, J. Atkinson, S. Gulesserian, P.M. Challita-Eid, S. Karki, F. Doñate

Other (design and implementation of in vitro cell based assays in human corneal epithelial cells to evaluate mechanism of ADCs mediate nonspecific cytotoxicity): Z. Zeng

Other (design and generation of original AGS-16C3F DNA construct, along with the design and generation of all site-directed mutagenesis variants): F. Malik

Acknowledgments

This study was funded by Agensys, Inc., an affiliate of Astellas Pharma. The authors thank all other members of Agensys who contributed to this study and did not appear on this article, in particular, Yuriy Shostak and Mi Sook Chang for supporting RNA expression analysis studies, Banmeet Anand for pharmacokinetic analysis, and Michelle Wu and Christopher Kemball for some of the HCEC *in vitro* data.

The costs of publication of this article were defrayed in part by the payment of page charges. This article must therefore be hereby marked *advertisement* in accordance with 18 U.S.C. Section 1734 solely to indicate this fact.

Received October 18, 2017; revised December 19, 2017; accepted January 25, 2018; published first January 30, 2018.

References

1. Beck A, Goetsch L, Dumontet C, Corvaia N. Strategies and challenges for the next generation of antibody-drug conjugates. Nat Rev Drug Discov 2017;16:315–37.
2. de Goeij BE, Lambert JM. New developments for antibody-drug conjugate-based therapeutic approaches. Curr Opin Immunol 2016; 40:14–23.
3. Donaghy H. Effects of antibody, drug and linker on the preclinical and clinical toxicities of antibody-drug conjugates. MAbs 2016;8:659–71.
4. Saber H, Leighton JK. An FDA oncology analysis of antibody-drug conjugates. Regul Toxicol Pharmacol 2015;71:444–52.
5. Zhao H, Gulesserian S, Malinao MC, Ganesan SK, Song J, Chang MS, et al. A Potential mechanism for ADC-induced neutropenia: role of neutrophils in their own demise. Mol Cancer Ther 2017;16:1866–76.
6. Zhao H, Gulesserian S, Ganesan SK, Ou J, Morrison K, Zeng Z, et al. Inhibition of megakaryocyte differentiation by antibody-drug conjugates (ADCs) is mediated by macropinocytosis: implications for ADC-induced thrombocytopenia. Mol Cancer Ther 2017;16:1877–86.
7. Eaton JS, Miller PE, Mannis MJ, Murphy CJ. Ocular adverse events associated with antibody-drug conjugates in human clinical trials. J Ocul Pharmacol Ther 2015;31:589–604.
8. Thompson JA, Motzer R, Molina AM, Choueiri TK, Heath EI, Kollmannsberger CK, et al. Phase I studies of anti-ENPP3 antibody drug conjugates (ADCs) in advanced refractory renal cell carcinomas (RRCC). J Clin Oncol 33, 2015 (suppl; abstr 2503).
9. Ribrag V, Dupuis J, Tilly H, Morschhauser F, Laine F, Houot R, et al. A dose-escalation study of SAR3419, an anti-CD19 antibody maytansinoid conjugate, administered by intravenous infusion once weekly in patients with relapsed/refractory B-cell non-Hodgkin lymphoma. Clin Cancer Res 2014;20:213–20.
10. Tannir NM, Forero-Torres A, Ramchandren R, Pal SK, Ansell SM, Infante JR, et al. Phase I dose-escalation study of SGN-75 in patients with CD70-positive relapsed/refractory non-Hodgkin lymphoma or metastatic renal cell carcinoma. Invest New Drugs 2014;32:1246–57.
11. Tsuda M, Takano Y, Shigeyasu C, Imoto S, Yamada M. Abnormal corneal lesions induced by trastuzumab emtansine: an antibody-drug conjugate for breast cancer. Cornea 2016;35:1378–80.
12. Beeram M, Krop IE, Burris HA, Girish SR, Yu W, Lu MW, et al. A phase 1 study of weekly dosing of trastuzumab emtansine (T-DM1) in patients with advanced human epidermal growth factor 2-positive breast cancer. Cancer 2012;118:5733–40.
13. Hassan R, Thomas A, Alewine C, Le DT, Jaffee EM, Pastan I. Mesothelin immunotherapy for cancer: ready for prime time? J Clin Oncol 2016;34: 4171–9.
14. Moore KN, Martin LP, O'Malley DM, Matulonis UA, Konner JA, Perez RP, et al. Safety and activity of mirvetuximab soravtansine (IMGN853), a folate receptor alpha-targeting antibody-drug conjugate, in platinum-resistant ovarian, fallopian tube, or primary peritoneal cancer: a phase I expansion study. J Clin Oncol 2017;35:1112–8.
15. Shapiro GI, Vaishampayan UN, LoRusso P, Barton J, Hua S, Reich SD, et al. First-in-human trial of an anti-5T4 antibody-monomethylauristatin conjugate, PF-06263507, in patients with advanced solid tumors. Invest New Drugs 2017;35:315–23.
16. Liu Z, Carvajal M, Carraway CA, Carraway K, Pflugfelder SC. Expression of the receptor tyrosine kinases, epidermal growth factor receptor, ErbB2, and ErbB3, in human ocular surface epithelia. Cornea 2001;20:81–5.
17. Bialucha CU, Collins SD, Li X, Saxena P, Zhang X, Durr C, et al. Discovery and optimization of HKT288, a cadherin-6-targeting ADC for the treatment of ovarian and renal cancers. Cancer Discov 2017;7:1030–45.
18. Coveler AL, Ko AH, Catenacci DV, Von Hoff D, Becerra C, Whiting NC, et al. A phase 1 clinical trial of ASG-5ME, a novel drug-antibody conjugate targeting SLC44A4, in patients with advanced pancreatic and gastric cancers. Invest New Drugs 2016;34:319–28.
19. Secker GA, Daniels JT. Limbal epithelial stem cells of the cornea. In: Watt F, Gage F, editors. StemBook [monograph on the Internet]. Cambridge (MA): Harvard Stem Cell Institute; 2008. Published 2009 Jun 30. Available from: https://www.ncbi.nlm.nih.gov/books/NBK27054/.
20. Joe AW, Yeung SN. Concise review: identifying limbal stem cells: classical concepts and new challenges. Stem Cells Transl Med 2014;3:318–22.
21. Doñate F, Raitano A, Morrison K, An Z, Capo L, Avina H, et al. AGS16F is a novel antibody drug conjugate directed against ENPP3 for the treatment of renal cell carcinoma. Clin Cancer Res 2016;22:1989–99.
22. Challita-Eid PM, Satpayev D, Yang P, An Z, Morrison K, Shostak Y, et al. Enfortumab vedotin antibody-drug conjugate targeting nectin-4 is a highly potent therapeutic agent in multiple preclinical cancer models. Cancer Res 2016;76:3003–13.
23. Mattie M, Raitano A, Morrison K, Morrison K, An Z, Capo L, et al. The discovery and preclinical development of ASG-5ME, an antibody-drug conjugate targeting SLC44A4-positive epithelial tumors including pancreatic and prostate cancer. Mol Cancer Ther 2016;15:2679–87.
24. Commisso C, Davidson SM, Soydaner-Azeloglu RG, Parker SJ, Kamphorst JJ, Hackett S, et al. Macropinocytosis of protein is an amino acid supply route in Ras-transformed cells. Nature 2013;497:633–7.
25. Lim JP, Gleeson PA. Macropinocytosis: an endocytic pathway for internalising large gulps. Immunol Cell Biol 2011;89:836–43.
26. Lloyd JB. Cell physiology of the rat visceral yolk sac: a study of pinocytosis and lysosome function. Teratology 1990;41:383–93.
27. Hawe A, Sutter M, Jiskoot W. Extrinsic fluorescent dyes as tools for protein characterization. Pharm Res 2008;25:1487–99.
28. Turecek PL, Bossard MJ, Schoetens F, Ivens IA. PEGylation of biopharmaceuticals: a review of chemistry and nonclinical safety information of approved drugs. J Pharm Sci 2016;105:460–75.
29. Lyon RP, Bovee TD, Doronina SO, Burke PJ, Hunter JH, Neff-LaFord HD, et al. Reducing hydrophobicity of homogeneous antibody-drug conjugates improves pharmacokinetics and therapeutic index. Nat Biotechnol 2015; 33:733–5.
30. King HD, Dubowchik GM, Mastalerz H, Willner D, Hofstead SJ, Firestone RA, et al. Monoclonal antibody conjugates of doxorubicin prepared with branched peptide linkers: inhibition of aggregation by methoxytriethyleneglycol chains. J Med Chem 2002;45:4336–43.
31. Igawa T, Tsunoda H, Tachibana T, Maeda A, Mimoto F, Moriyama C, et al. Reduced elimination of IgG antibodies by engineering the variable region. Protein Eng Des Sel 2010;23:385–92.
32. Wilson SL, Ahearne M, Hopkinson A. An overview of current techniques for ocular toxicity testing. Toxicology 2015;327:32–46.